

On the capillary self-focusing in a microfluidic system

M. Hein¹, R. Seemann¹ ‡, and S. Afkhami² §

¹ Experimental Physics, Saarland University, 66123 Saarbrücken, Germany

² Department of Mathematical Sciences, New Jersey Institute of Technology, Newark, NJ 07102, USA

Abstract. A computational framework is developed to address capillary self-focusing in Step Emulsification. The microfluidic system consists of a single shallow and wide microchannel that merges into a deep reservoir. A continuum approach coupled with a volume of fluid method is used to model the capillary self-focusing effect. The original governing equations are reduced using the Hele–Shaw approximation. We show that the interface between the two fluids takes the shape of a neck narrowing in the flow direction just before entering the reservoir, in agreement with our experimental observations. Our computational model relies on the assumption that the pressure at the boundary, where the fluid exits into the reservoir, is the uniform pressure in the reservoir. We investigate this hypothesis by comparing the numerical results with experimental data. We conjecture that the pressure boundary condition becomes important when the width of the neck is comparable to the depth of the microchannel. A correction to the exit pressure boundary condition is then proposed, which is determined by comparison with experimental data. We also present the experimental observations and the numerical results of the transitions of breakup regimes.

Keywords: Microfluidics, Step Emulsification, Capillary Focusing, Hele–Shaw, Volume Of Fluid Simulation

‡ Corresponding author: r.seemann@physik.uni-saarland.de

§ Corresponding author: shahriar.afkhami@njit.edu

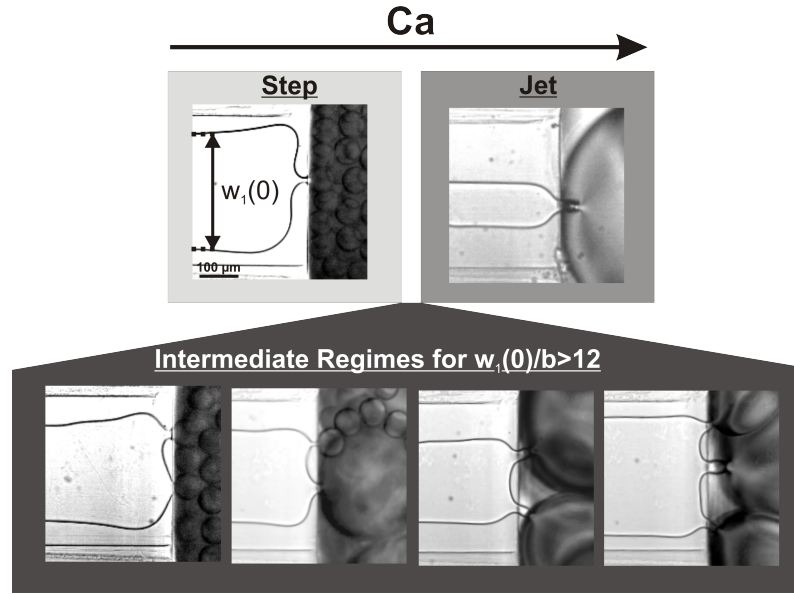


Figure 1. Breakup regimes observed in step emulsification droplet generation. At low $w_1(0)/b$, with b the depth of the shallow channel, the step and the jet emulsification regimes are observed for low and high capillary numbers, Ca , respectively. Insert: For $w_1(0)/b > 12$, the coexistence of multiple breakup sites on a single filament is observed.

1. Introduction: Background and the Mathematical Model

Step emulsification is a microfluidic technique for generating monodisperse droplets with highly controllable sizes and production rates (Priest *et al* 2006). The process relies on breakup of a long and wide confined sheet of fluid, surrounded by a second fluid, at a step geometry, consisting of a single shallow and wide microchannel that abruptly merges into a deep reservoir (see Fig. 1). At the step, the interface between the two fluids takes the shape of a tongue narrowing in the flow direction; we call this the capillary self-focusing. When the self-focused pointed tongue enters into the reservoir, the interface becomes unstable resulting in the formation of droplets at the step. This can be explained by the fact that in the focusing region, a cylindrical thread is formed and becomes unstable by the resulting lack of confinement, as it enters the reservoir, presumably by a Rayleigh-Plateau instability mechanism (Li *et al* 2015). Previously, we showed that the width of this focusing region is directly related to the transition of breakup regimes (Hein *et al* 2015a), namely the jet- and step-breakup regimes, where the breakup transitions from a quasi-steady (jet-breakup) to a transient (step-breakup) regime (see Fig. 1 top panels). Here, we aim to extend our investigation of this self-focusing phenomena and our understanding by comparing the numerical results with experimental observations.

We adopt the classical steady Hele-Shaw flow equations, which is a simple description of the flow of a viscous Newtonian liquid between two horizontal plates

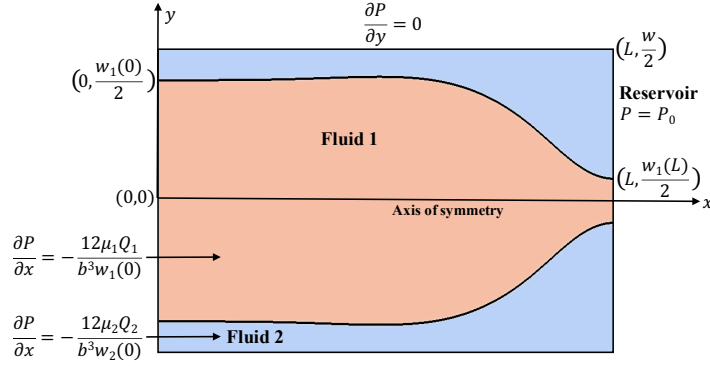


Figure 2. Schematic of the flow domain and the corresponding boundary conditions for the Hele–Shaw cell of width w .

separated by a thin gap, with surface tension

$$\mathbf{u}(x, y, t) = \frac{[b(x, y)]^2}{12\mu(f(x, y, t))} \{-\nabla P(x, y, t) + \gamma\kappa\delta_S\hat{\mathbf{n}}\}, \quad (1)$$

where $\mu(f(x, y, t))$ is the viscosity, $b(x, y)$ the depth of the Hele–Shaw cell, $P(x, y, t)$ the local pressure, δ_S the interface Dirac delta function, κ the in-plane curvature, γ the interfacial surface tension, and $\hat{\mathbf{n}}$ the unit normal. $f(x, y, t)$ is the volume of fluid function defined as 1 inside fluid 1 and 0 inside fluid 2, for a two fluid system (see Fig. 2). The evolution of $f(x, y, t)$ satisfies the advection equation

$$\partial_t f(x, y, t) + \nabla \cdot (\mathbf{u}(x, y, t)f(x, y, t)) = 0. \quad (2)$$

The numerical discretization and validations are described in detail in (Afkhani and Renardy 2013). This simplified model can significantly reduce the computational cost and complexity, while allowing to keep the essential features of the flow. Furthermore, our computational model relies on the assumption that the pressure at the boundary, where the fluid exits into the reservoir, is the uniform pressure in the reservoir. This hypothesis is computationally investigated by comparing the numerical results with the experimental measurements. In particular, we conjecture that the pressure boundary condition becomes important when the width of the neck is comparable to the depth of the microchannel. A correction to the pressure boundary condition at the outflow is then proposed, relying only on a single free parameter, which remains to be determined by comparison to experimental data.

2. Results and Discussion

We present the experimental observations and the numerical results based on the Hele–Shaw approximation combined with a volume of fluid method for computing the interface motion and for modeling the surface tension. Figure 2 shows a schematic of the flow domain and the corresponding boundary conditions used in the numerical model. For

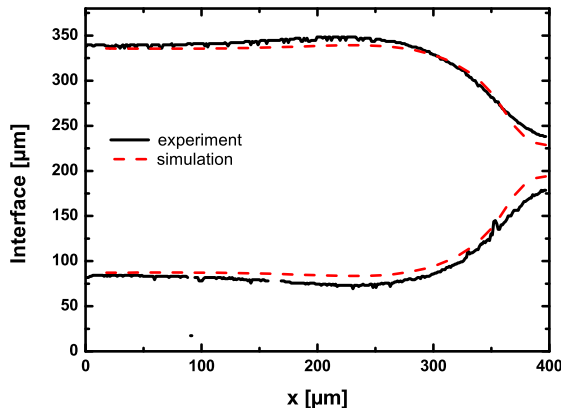


Figure 3. Comparison of the numerical results with the experiment for $Ca = b^2 [dp_1/dx]_{x=0} / (12\gamma) = 0.019$ and $w_1(0)/b = 12.76$, when $A = 1$.

all the results here, we fix the viscosity ratio to 1 and set the same pressure gradient for each phase at the inlet ($x = 0$). We also fix $b(x, y) = b$. Experimental results in (Priest *et al* 2006) and (Hein *et al* 2015b) show that the transition of jet- to step-breakup regime is independent of the viscosity ratio when the results are presented in terms of the rescaled filament width $w_1(0)/b$ as a function of Ca . We therefore do not consider unmatched viscosities in this work. To model the reservoir, we set a zero pressure (P_0 is the reference pressure in the reservoir) at the outlet ($x = L$). We account for the influence of the growing three-dimensional droplet in the reservoir and the reservoir itself with a simple pressure boundary condition at where the fluid exits into the reservoir. Specifically, the outflow pressure boundary condition is defined as

$$P(L, y, t) = \begin{cases} P_0 + A(2\gamma/b) & -w_1(L)/2 \leq y \leq w_1(L)/2 \\ P_0 & \text{otherwise} \end{cases} \quad (3)$$

where A is the pressure correction parameter and the out-of-plane curvature is assumed to be constant and equal to $2/b$, i.e. $2\gamma/b$ represents the Laplace pressure at the neck ($x = L$). Next, we examine this simple pressure boundary condition in both the jet-breakup regime, where $w_1(L) \gg b$, and close to the transition to step-breakup regime, where $w_1(L) \sim b$. We will show that the pressure correction is needed, when close to the transition to step-breakup regime, for reasonable agreement with physical experiments. We however note that since the pressure beyond the step is unknown, we can only speculate either the inflating three-dimensional drop in the reservoir or the out-of-plane curvature to be the physical origin of the pressure correction. We leave a thorough study of these effects, including fully three-dimensional computations, for future work.

Figure 3 shows the computationally predicted interfacial profile, in the (single) jet-breakup regime, in comparison with the experimental measurement for $A = 1$, i.e. assuming no correction to the pressure boundary condition at the exit. As shown, a very good agreement with experimental visualization is obtained. Next, we will consider

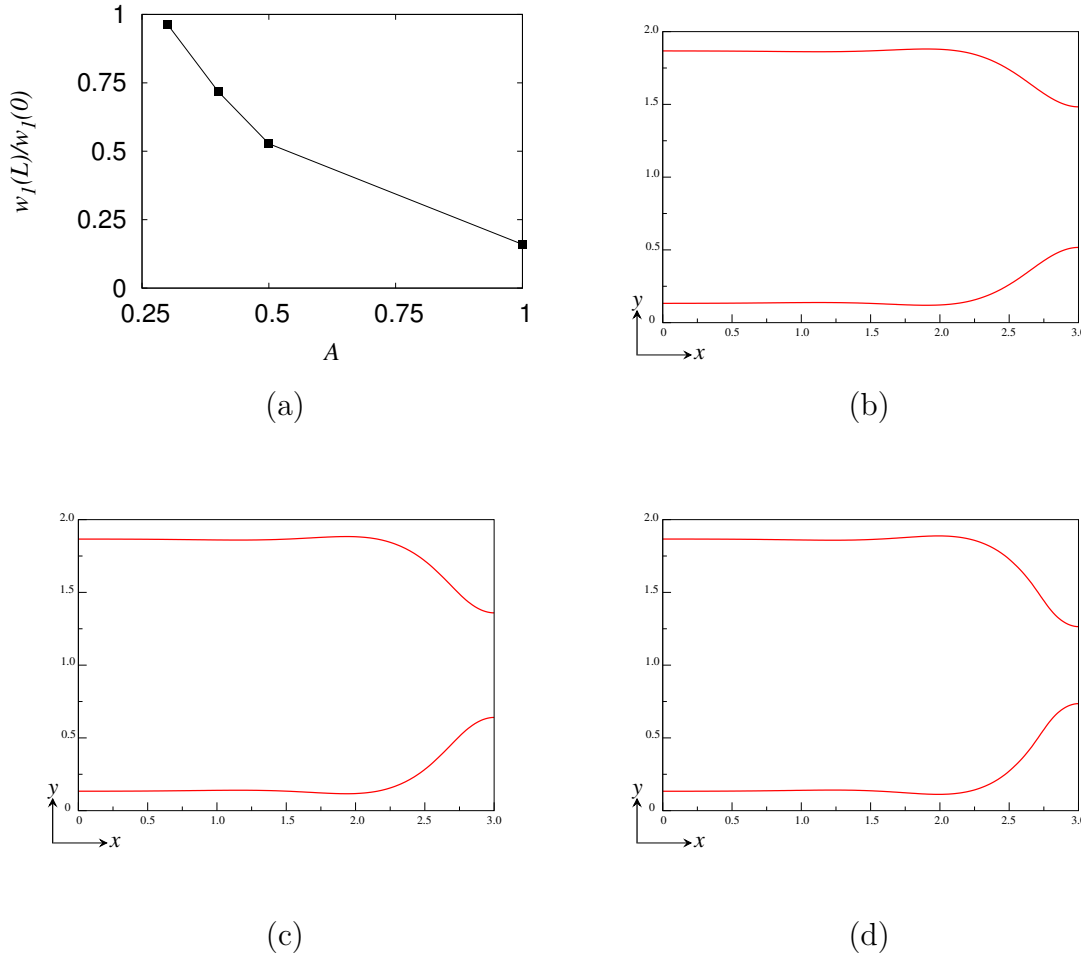


Figure 4. (a) $w_1(L)/w_1(0)$ as a function of A . The shape of the capillary focusing with (b) $A = 0.3$, (c) 0.4 , and (d) 0.5 . The neck widens as A is decreased. For these simulations $Ca = 0.01$ and $w_1(0)/b = 10$.

the breakup regime close to the transition from jet- to the step-breakup. We are going to define the transition of the jet-breakup to the step-breakup as when the dispersed phase forms a circular jet upon exiting into the reservoir. In reality, this should happen when $w_1(L) \approx b$, because the dispersed phase will become unstable below this width due to the Rayleigh-Plateau type of instability. Thus, in practice, $w_1(L) \approx b$ is the smallest achievable width of the focusing neck. In the following, we will discuss in more detail the effect of the pressure correction, A , on the focusing close to the transition from the jet- to step-breakup regime.

Figure 4(a) presents the width of the focusing neck at the exit, $w_1(L)$, normalized by width of the dispersed phase at the inlet, $w_1(0)$, as a function of the pressure correction, A . The results show that decreasing the pressure in the dispersed phase at the step by a factor 3 results in an increase in $w_1(L)$ by a factor of 6. We therefore show that the pressure boundary condition can play an important role when the width of the

focusing neck becomes comparable to the depth of the channel. Figures 4(b-d) show the shape of the capillary focusing for three different pressure correction parameters used in Fig. 4(a). As demonstrated, the capillary focusing becomes less pronounced with a decrease of the pressure in the dispersed phase at the exit. We note again that when $A = 1$, the pressure inside the dispersed phase at the exit boundary is just $2\gamma/b$, i.e. the Laplace pressure of a meniscus of mean curvature $2/b$.

As in (Hein *et al* 2015a), we define the critical Ca number as the capillary number for which the jet-breakup transitions to a step-breakup for a fixed $w_1(0)/b$. As discussed above, and shown experimentally in (Hein *et al* 2015a), this transition occurs when $w_1(L) \approx b$. For $w_1(0)/b = 10$, the experiments of (Hein *et al* 2015a) finds the critical $\text{Ca} \lesssim 0.005$. We next investigate whether we can find an A that permits $w_1(L) \approx b$ for $w_1(0)/b = 10$ at Ca close to the experimentally observed transition from jet- to step-breakup regime. For each A , we vary the Ca number to obtain the value of Ca for which $w_1(L) \approx b$. We find that only for $A = 0.4$, we can obtain $w_1(L) \approx b$ for $\text{Ca} = 0.004$. From this analysis, we can infer that the transition from jet- to step-breakup is reached at $\text{Ca} = 0.004$ only if the corrected pressure boundary condition at the outflow is employed. This corrected pressure boundary condition corresponds to a significantly smaller Laplace pressure inside the dispersed phase at the exit, which could be the consequence of a smaller out-of-plane curvature than considered when $A = 1$; i.e. $2/b$. One possible physical explanation can be that in the step-breakup regime, upon the formation, the droplet is initially confined and rapidly ‘feels’ the reservoir, causing it to assume a smaller out-of-plane curvature than $2/b$. We therefore conjecture that the capillary focusing is strongly sensitive to the values of the considered out-of-plane curvatures at the exit, and therefore the discrepancy between the numerical results and the experimental data is most likely explained through this sensitivity. We thus show that our correction to the outflow pressure boundary condition can be an effective way to achieve numerical results that agree reasonably well with experimental measurements, without resorting to fully three-dimensional simulations.

However, the precise prediction of the critical Ca number (i.e. the Ca for which $w_1(L) \approx b$), by introducing the pressure correction A , comes with the expense of a reduced focusing effect. Figure 5(a) shows that we obtain $w_1(L) \approx b$ for $\text{Ca} = 0.01$ when $A = 1$ and for $\text{Ca} = 0.004$ when $A = 0.4$. We remind that in (Hein *et al* 2015a), the breakup regime transition is reported to occur at $\text{Ca} \lesssim 0.005$. Figure 5(a) shows that the focusing effect is much stronger when $A = 1$ and $\text{Ca} = 0.01$ than when $A = 0.4$ and $\text{Ca} = 0.004$. This is somehow counterintuitive. It shows that if we do not consider any pressure correction at the outflow, i.e. $A = 1$, a much larger Ca must be attained in order to obtain $w_1(L) \approx b$, leading to a more profound capillary focusing effect. Figure 5(b) demonstrates the local change of the interface shape in the focusing region by plotting the computed interface curvature for $\text{Ca} = 0.01$ and $A = 1$, and for $\text{Ca} = 0.004$ and $A = 0.4$. The results show the abrupt change in the curvature in the narrowing region; curvature becomes negative in the focusing region. As shown, the increase in the capillary number results in the decrease of the length scale over which the curvature

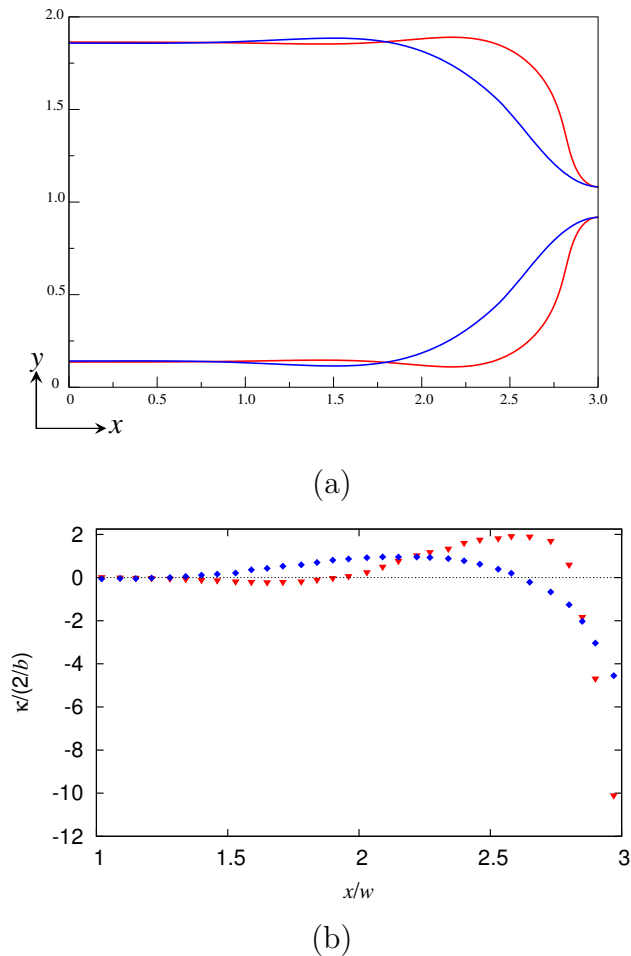


Figure 5. (a) The shape of the capillary focusing for $Ca = 0.01$ with no pressure boundary condition correction at the outflow, $A = 1$ (red), and for $Ca = 0.004$ with a pressure boundary condition correction at the outflow, $A = 0.4$ (blue); $w_1(L) \approx b$. (b) Computed interface curvature normalized by $2/b$, the magnitude of the curvature at the outflow ($x = L$), as a function of x/w for $Ca = 0.01$ and $A = 1$ (\blacktriangledown), and for $Ca = 0.004$ and $A = 0.4$ (\blacklozenge); the dashed line, $\kappa = 0$, is plotted for visual assistance for when the curvature changes sign. $w_1(0)/b = 10$.

changes sign, i.e. the focusing region length scale. We also note that with $A = 1$, we arrive at $\kappa = -2/b$ at the outlet ($x = L$), while smaller A results in a smaller Laplace pressure at the outlet.

2.1. Transitions of breakup regimes

In (Hein *et al* 2015b), multiple breakup regimes are addressed. In their work, the authors show that, when $w_1(0)/b \gtrsim 12$, a variety of breakup regimes can be observed depending on the Ca number. For example, they show that when $w_1(0)/b$ is fixed and $w_1(0)/b \gtrsim 15$, a double jet-breakup can occur, for a particular range of small

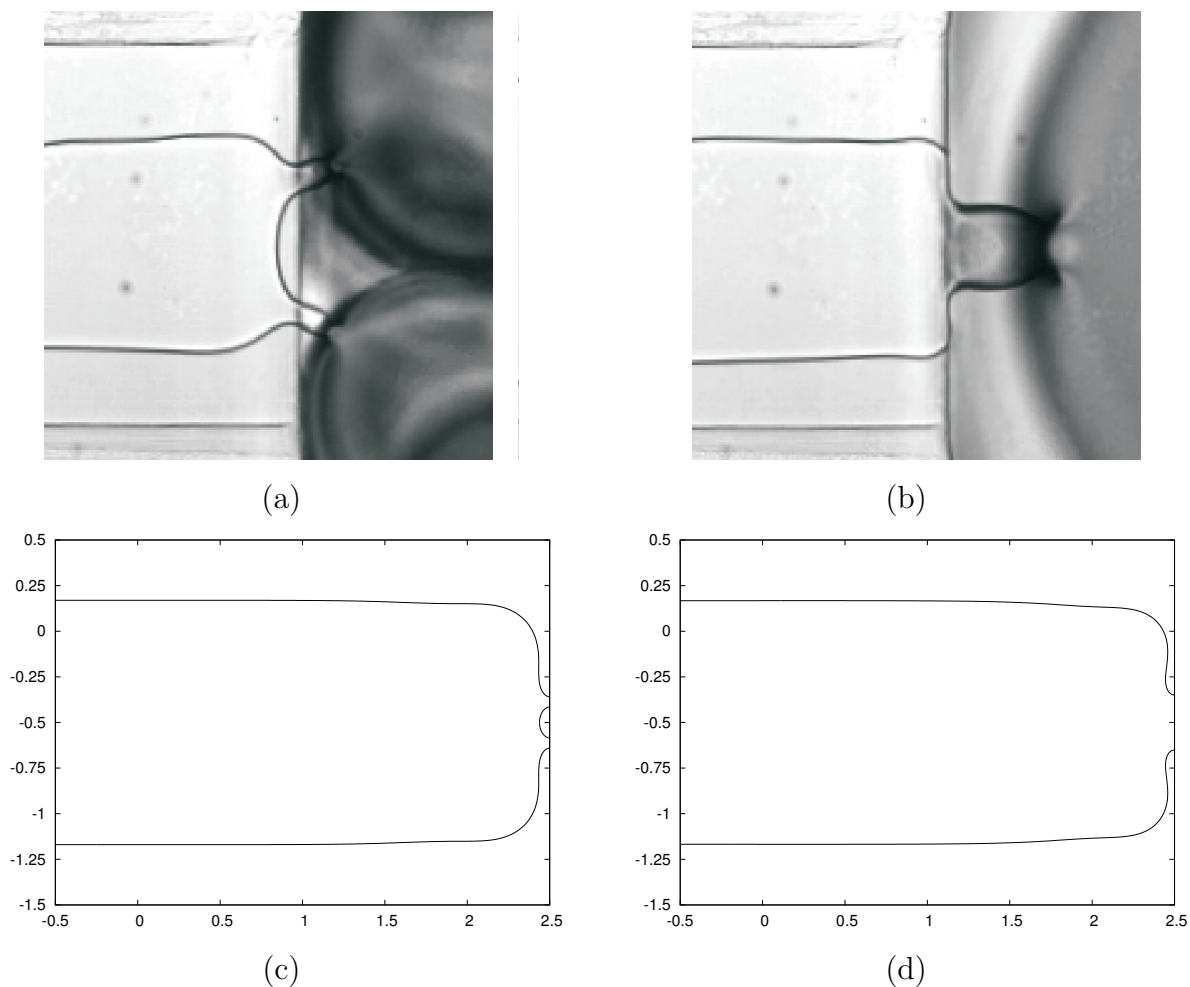


Figure 6. It is shown that a double jet-breakup can occur depending on $w_1(0)/b$ and the Ca number. For a fixed $w_1(0)/b$, increasing Ca number results in collapsing of double jets into a single jet. Optical micrographs showing two regimes of droplet breakup; (a) a double jet-breakup for $Ca = 0.0223$ and $w_1(0)/b = 16.4$ and (b) a single jet-breakup for $Ca = 0.039$ and $w_1(0)/b = 19.6$. Simulations showing (c) a double jet-breakup for $Ca = 0.0125$ and (d) a single jet-breakup for $Ca = 0.025$; $w_1(0)/b = 20$. For these results $w/b = 30$.

Ca numbers, which collapses into a single jet-breakup by increasing the Ca number. In Fig. 6(a-b), we show the experimental observation of these two breakup scenarios. We attribute the double jet-breakup to the strong confinement. The transition from double to single jet-breakup is discussed in details in (Hein *et al* 2015b). Here we also numerically show the existence of these breakup regimes. Figures 6(c-d) show simulation results of different breakup regimes for $Ca = 0.0125$ (double jet-breakup) and $Ca = 0.025$ (single jet-breakup) when $w_1(0)/b = 20$. This transition is in agreement with our experiments previously documented in (Hein *et al* 2015b). For these simulations, we use $A = 1$. These unprecedented results provide excellent insight into the capillary self-focusing phenomena, capturing multiple breakup regimes using our simple pressure

boundary condition. The numerical results shown in Figs. 6(c-d) also exhibit the strong capillary focusing effect when increasing confinement. Figure 6(d) shows that the front of the filament is almost flat at the exit, in agreement with the profile in Fig. 6(b). Upon decreasing the Ca number, i.e. increasing the capillary focusing effect, such a wide and flat interface allows easy formation of another jet at the exit (Fig. 6(c)). Our experiments show that for a double jet-breakup, droplets that are formed in the reservoir (see Fig. 6(a)) grow and elongate while traveling downstream; during this elongation, the two tips formed at the step are pushed outwards. The absence of this effect explains the difference in the location of the two tips which are more centered in the simulation.

3. Conclusions

We confirm the validity of our numerical simulations, based on the classical Hele–Shaw formulation and a simple pressure boundary condition at which the fluid exits into the reservoir, by comparing with experimental results. Despite the inherent assumptions, the computational framework describes the capillary self-focusing consistently with our experimental findings. For the jet-breakup regime and sufficiently large Ca numbers, we show that the numerical model well captures the focusing profile without any correction to the pressure boundary condition. Close to the transition from a jet-breakup regime to a step-breakup regime, a pressure correction is required in order to predict the transition threshold. The correction is most likely due to the effects of the expanding three-dimensional droplet in the reservoir or an out-of-plane curvature that becomes smaller than $2/b$ because of the sudden relief of the confinement at the step, or a combination of these. For further consideration of these effects, fully three-dimensional computations are needed. We leave this extension for future work.

We also conjecture that the pressure boundary condition becomes important when the width of the focusing region is comparable to the depth of the shallow microchannel. The corrected pressure boundary condition at the outflow takes into account a single free parameter, to be determined by comparison with experimental data. Our numerical results also provide an excellent insight into the capillary self-focusing phenomena when there exists a strong confinement. In particular, consistently with our experimental results, we show that our numerical simulations can identify a double jet-breakup regime and its transition to a single jet-breakup regime upon decreasing the confinement or increasing the Ca number. Ongoing work in microfluidics drop generation makes our results highly relevant for technical applications. For example, for droplet based microfluidic systems (see e.g. Seemann *et al* 2012), when using channel geometries such as the ones in this work, the occurrence of multiple breakup sites at a topographic step on the same filament will be likely or even desired, e.g. for the simultaneous particle or cell encapsulation or filtering, providing a novel tool in the droplet microfluidics applications.

Acknowledgments

This work was partially supported by the grant Nos. DFG-GRK1276 and NSF-DMS-1320037. Authors gratefully acknowledge Dr. Jean-Baptiste Fleury (Saarland University) for helpful discussions.

References

- Priest C, Herminghaus S, and Seemann R 2006 Generation of monodisperse gel emulsions in a microfluidic device *Appl. Phys. Lett.* **88** 024106
- Malloggi F, Pannacci N, Attia R., Monti F, Mary P, Willaime H, Tabeling P, Cabane B, and Poncet P 2010 Monodisperse Colloids Synthesized with Nanofluidic Technology *Langmuir* **26** 2369-2373
- Afkhami S and Renardy Y 2013 A volume-of-fluid formulation for the study of co-flowing fluids governed by the Hele–Shaw equations *Phys. Fluids* **25** 082001
- Hein M, Afkhami S, Seemann R, and Kondic L 2015a Capillary focusing close to a topographic step: shape and instability of confined liquid filaments *Microfluid. Nanofluid.* **18** 911-917
- Li Z, Leshansky A, Pismen L, and Tabeling P 2015 Step-emulsification in a microfluidic device *Lab Chip* **15** 1023-1031
- Hein M, Fleury J-B, and Seemann R 2015b Coexistence of different droplet generating instabilities: new breakup regimes of a liquid filament *Soft Matter* **11** 5246-5252
- Seemann R, Brinkmann M, Pfohl T, and Herminghaus S 2012 Droplet based microfluidics *Rep. Prog. Phys.* **75** 016601.